CHAPTER 6

EFFECT OF PRE-HOT CORROSION ON EROSION BEHAVIOUR OF TYPE 446 STAINLESS STEEL

6.1 INTRODUCTION

The power plant units are routinely set for maintenance after a specified cycle of operation. During this maintenance period or even during the breakdown period, the heat exchanger tubes undergo corrosion due to residues fluid deposited on the inner surface of the tubes. These fluids contain corrosive species like Na_2SO_4 and NaCl which are responsible for corrosion and surface degradation. The problems arising due to the synergistic effect of corrosion enhanced erosion are severe and their complexity is not thoroughly understood. Therefore, the pre-hot-corroded samples were exposed to erosion, to mimic the corrosion enhanced erosion behavior.

The present study deals with the influence of hot-corrosion enhanced solid particle erosion behavior of Type 446 stainless steel used in heat exchangers. The test specimens were hot-corroded using NaCl and Na_2SO_4 deposits by the spray deposition technique. The coating of two salt mixture (75 wt% Na_2SO_4 + 25 wt% NaCl) easily degrades the Cr_2O_3 protective layer, thereby, penetrating the salts through the protective layer. These salts when in contact with the matrix cause significant sulfidation [177]. Li et al. [178] highlighted that the unevenness of surface oxide film due to localized attack enhances crack growth. Eventually, detaching the oxide flakes to increased erosion. Both corrosion kinetics evolution and

morphological development are investigated by means of weight gain measurements, metallographic examination, and identification of the corrosion products. The mechanism responsible for deterioration of materials involved in corrosion enhanced erosion process are studied using XRD and SEM.

6.2 RESULTS

6.2.1 Macrographs of hot corroded samples

The hot corrosion scales were featured, using a digital camera, as shown in Fig. 6.1. The hot corroded samples exposed to 550℃ have an oxide layer with golden grey surface appearance having sketchy scaling and fewer pores (Fig. 6.1a), while at 650℃, the appearance is like chestnut with heavy scaling and spalling of the scale (Fig. 6.1b). Similarly, when exposed to 750℃, the surface appeared to be dim-grey in colour (Fig. 6.1c) with the formation and spalling of a fragile scale.

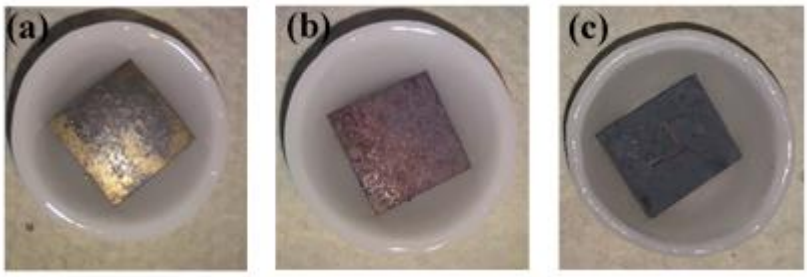

Fig. 6.1: Macrograph of hot corroded samples for 20 h at: **(a)** 550℃ **(b)** 650℃, and **(c)** 750℃

6.2.2 Weight gain of the corroded specimen

Salt coated specimens when exposed to 550℃ did not show any significant weight change. However, at 650 and 750℃, the marked increase in weight gain is recorded. This is evident from the bar chart (Fig. 6.2) which shows weight gain, against temperature, per unit area for a hot corroded sample.

 "© ASME Publishing. Reproduced with permission. All rights reserved"

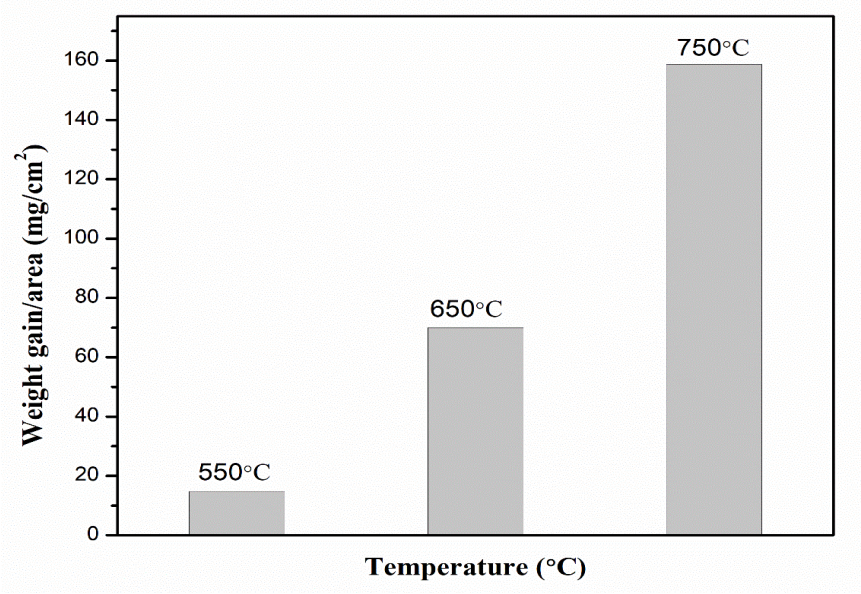

Fig. 6.2: Weight gain per unit area vs temperature showing the effect of hot corrosion at 550,650 and 750℃ for 20 h in air.

6.2.3 Diffusion of corrosive species

The coated samples after the hot corrosion test at 550, 650 and 750℃, for 20 h, were sectioned longitudinally from the centre of the sample. A passive layer of oxides and corrosive species is formed during the process of hot corrosion. Figure 6.3(a-c) shows the depth of attack of different corrosive species at 550, 650 and 750℃ respectively. The depth of attack was found maximum at 750℃, followed by 650℃, whereas, minimum attack of corrosive species is seen at 550℃. Figure 6.3(a) shows the cross-sectional view of the sample corroded at 750℃, with a number of crevices and a delaminated layer visible in the cross-section. On the other hand, at 650℃, the cracks developed in the corroded layer of iron oxide is clearly visible. This layer with numerous cracks emulates dry mud like structure with cracks initiating from the surface as shown in Fig. 6.3(b). Since eutectic temperature of the salt mixture is 628℃, therefore, the depth of attack was minimum at 550℃ (Fig. 6.3c).

 "© ASME Publishing. Reproduced with permission. All rights reserved"

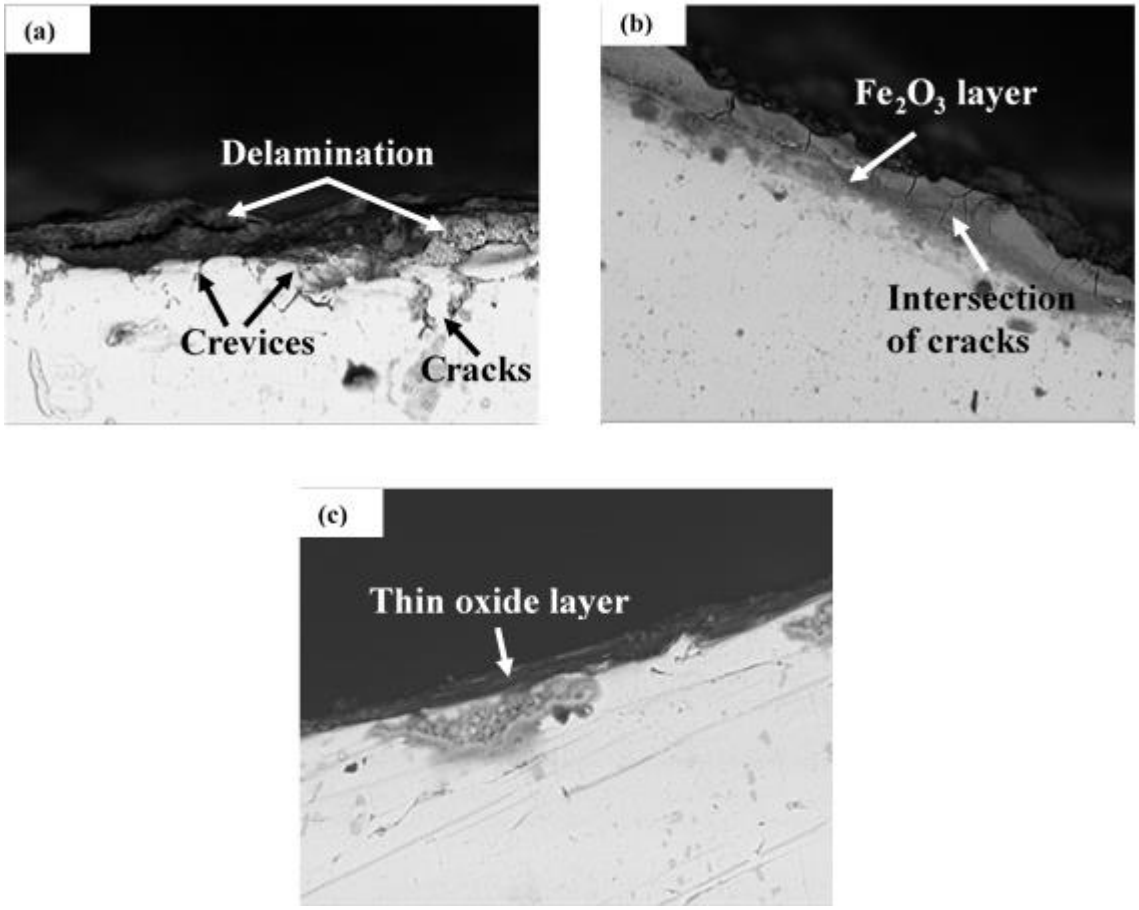

Fig. 6.3: SEM micrograph of cross-section of hot corroded samples showing the effect of diffusion of corrosive species at (a) 750℃ (b) 650℃ and (c) 550℃.

6.2.4 X-ray Diffraction analysis of hot corroded samples

The hot corrosion process is greatly influenced by the properties of the phases formed at elevated temperatures. The XRD patterns of the coated samples, with two salt mixture, after isothermal exposure of 20 h at different temperatures is shown in Fig. 6.4. Certain phases like Cr_2O_3, $FeCr_2O_4$, Fe_3O_4, Fe_2O_3, FeS_2 were identified.

6.2.5 Surface morphology and composition

The SEM micrograph of hot corroded samples reveals the non-uniformity in the surface feature of the oxide scales formed during corrosive species attack. Figure 6.5 represents the surface morphology of the sample corroded at 550℃, which clearly shows that there is a minor effect of the aggressive environment. However, samples corroded with two salt mixture at 650℃ for 20 h showed scales of flaky and cuboidal structures, which are

 "© ASME Publishing. Reproduced with permission. All rights reserved"

mainly the oxides of iron and chromium, shown in Fig. 6.6. EDS analysis of the top surface showed various elements complementary to their corresponding oxides. The formation of sago like spheroidal structure at 750°C represents mainly oxides of iron, (Fig. 6.7), as confirmed by EDS analysis.

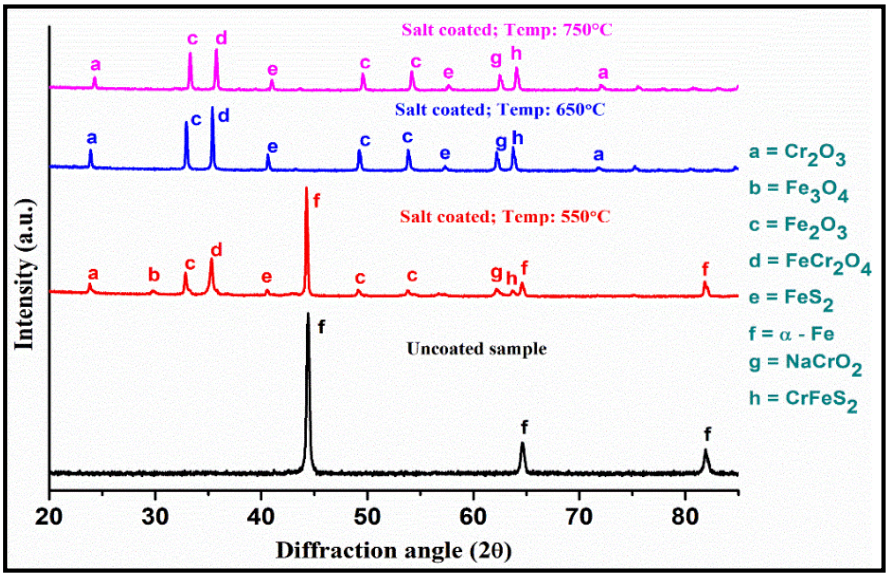

Fig. 6.4: XRD pattern of the oxides formed during hot corrosion of salt mixture coated sample in air for 20 h under variable temperature.

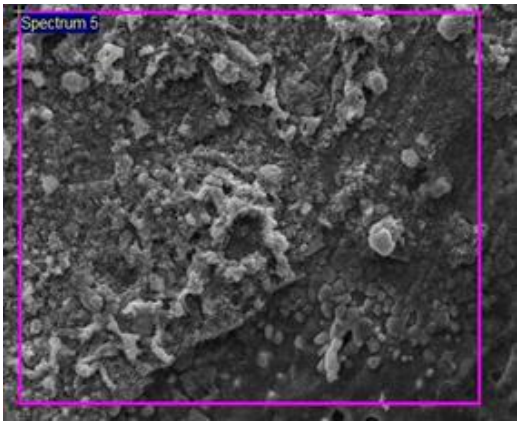

Elements	Weight %
O K	23.5
Na K	0.6
S K	0.3
Cl K	0.1
Cr K	19.9
Fe K	55.6

Fig. 6.5: SEM/EDX showing morphology and concentration of different elements of salt mixture deposited sample exposed at 550°C for 20 h.

 "© ASME Publishing. Reproduced with permission. All rights reserved"

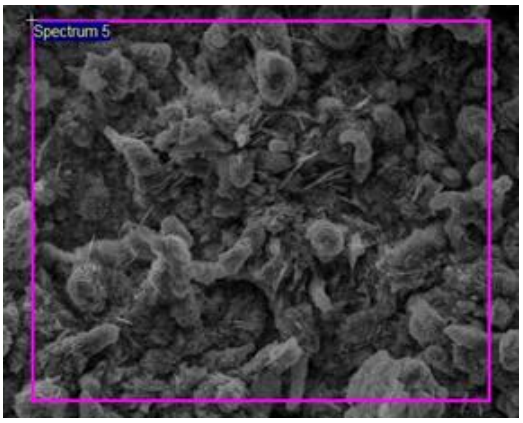

Elements	Weight %
O K	36.7
Na K	0.4
Cl K	0.1
Cr K	11.4
Fe K	61.4

Fig. 6.6: SEM/EDX showing morphology and concentration of different elements of salt mixture deposited sample exposed at 650℃ for 20 h.

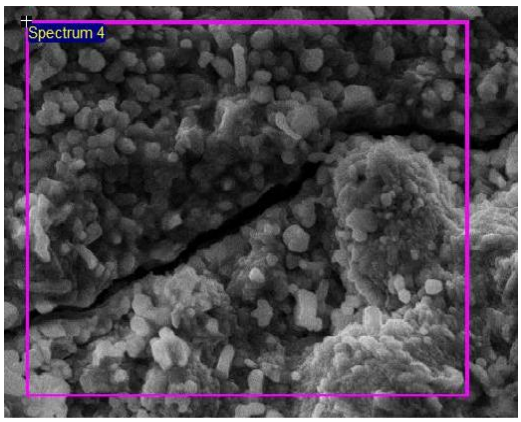

Elements	Weight %
O K	25.6
Na K	2.3
S K	0.6
Cr K	4.5
Fe K	67.0

Fig. 6.7: SEM/EDX showing morphology and concentration of different elements of salt mixture deposited sample exposed at 750℃ for 20 h.

6.2.6 Elemental mapping of the cross-section

The cross-sections of the hot corroded samples exposed at 650 and 750℃, for 20 h were examined by secondary electron (SE) x-ray mappings as shown in Figs. 6.8 and 6.9. The sample exposed at 750℃ experienced severe attack of hot corrosion as compared to samples corroded at 650℃, due to the formation of eutectic compounds [179]. Figure 6.8 shows the spalling, observed in dense oxide scales, which were formed at 750℃, whereas in case of samples corroded at 650℃, less dense layer of oxides (Fig. 6.9) was observed. It is worth mentioning that concentration of iron and oxygen is more in the corroded region and chromium is depleted forming a depleted region. This is due to the standard free energy of formation associated with chromium. The elements of iron

 "© ASME Publishing. Reproduced with permission. All rights reserved"

and chromium, on diffusion from the base material towards the surface, resulted in the formation of Fe_2O_3, Fe_3O_4, Cr_2O_3 oxides.

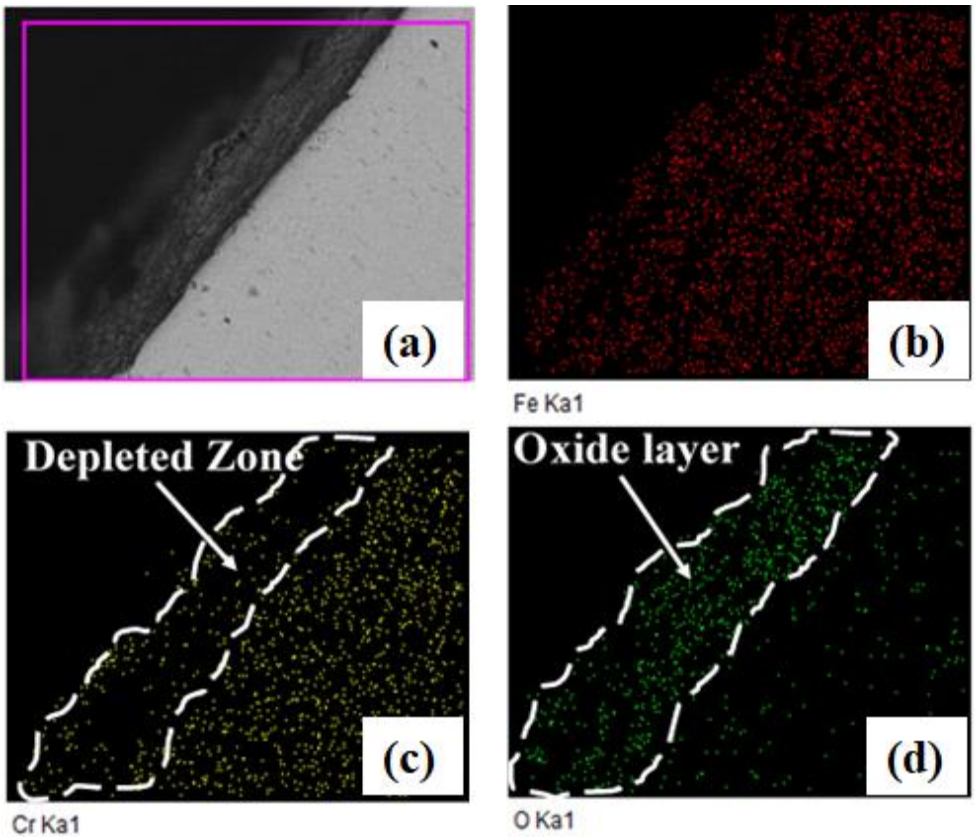

Fig. 6.8: Secondary electron X-ray mapping of cross-section of the two salt mixture deposited sample exposed at 750℃ for 20 h, focussing the elemental distribution **(a)** cross-section, **(b)** Iron, **(c)** Chromium, and **(d)** Oxygen.

6.2.7 High-temperature Erosion Wear

The hot corroded samples when subjected to erosion at high-velocity impacts, suffer higher material loss. At 550℃, the erosion rate is approximated same as that of the non-coated surface. Although, with an increase in temperature, the erosion rate is seen to increase to as large as three folds. On the contrary, under constant temperature conditions, the rate of erosion diminishes with an increase in angle of impact as shown in Fig. 6.10. This effect on erosion rate is attributed to the shear force acting on the surface and the products formed during corrosion. When subjected to higher test

 "© ASME Publishing. Reproduced with permission. All rights reserved"

temperature, the shallow angles of impact form protrusions which are easily removed under successive impacts, thereby, higher loss of the material is measured. Whereas for normal impacts, deformation wear is seen which is less significant to higher test temperature and thus erosion is reduced [180].

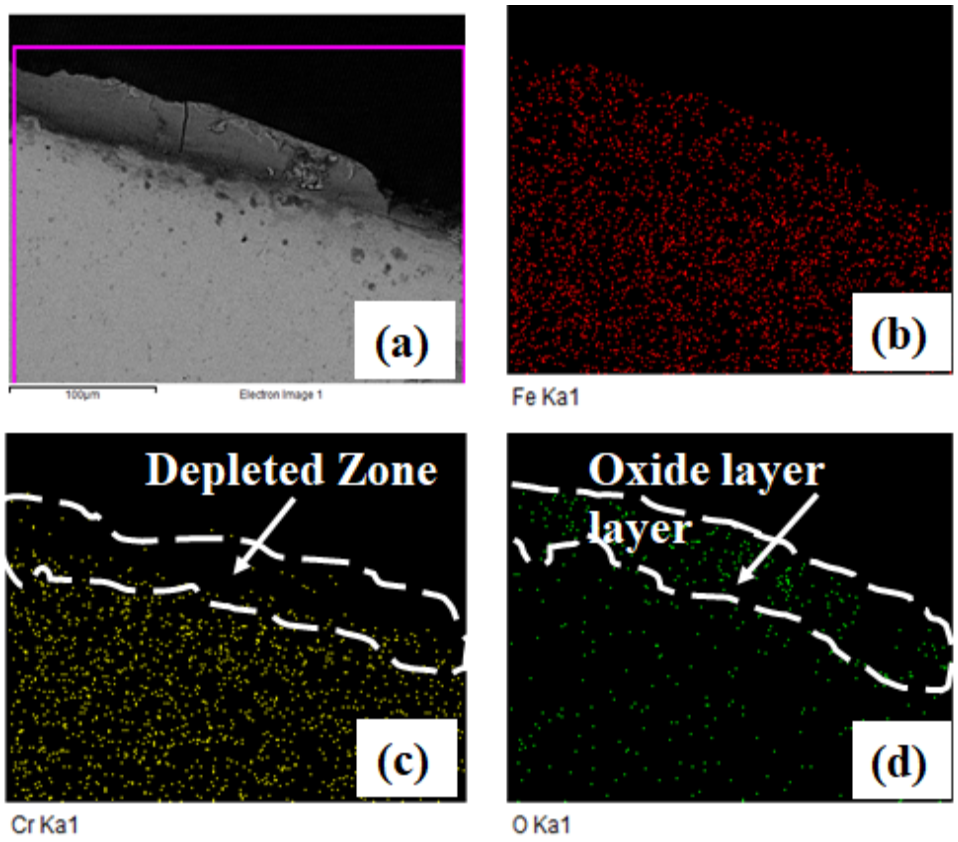

Fig. 6.9: Secondary electron X-ray mapping of cross-section of the two salt mixture deposited sample exposed at 650℃ for 20 h, focussing the elemental distribution **(a)** cross-section, **(b)** Iron, **(c)** Chromium, and **(d)** Oxygen.

The measurement carried out for 30° impact angle shows that after every 5 minutes of cycle time, erosion rate changes invariably at 550℃. Whereas, a common behaviour for test temperature of 650 and 750℃ shows a regular increment in erosion rate for an initial period of 20 minutes, thereafter a steady-state of erosion is recorded, as shown in Fig. 6.11. Erosion scar formed on the surface is observed to undergo significant change in profile, from the narrow elliptical groove at 30° to a deep hole at 90°. The

 "© ASME Publishing. Reproduced with permission. All rights reserved"

result of the depth of the scar at 90° impact is shown in Fig. 6.12. Erosion scar result is substantiated using laser profiling. At 90° impact angle, the shape of the worn scar is semi-spherical. The depth of this scar is measured from a reference plane to the deepest point within the damaged zone. However, the face of the sample subjected to impact is non-uniform and the elevation gradient is clearly reflected. This is due to the pre-hot corrosion effect under which the corrosive species react unevenly creating elevations and depressions on the surface.

When observed through a cross-sectional plane passing through the centre of the scar, it is seen that the erosion scar is elliptical in shape, therefore, random data points along the major axis and minor axis are chosen in X and Y direction as shown in Fig. 6.13. Whereas, within the scar region the measurement recorded a maximum depth of 209 µm. The values at different points along the plane are given in Table 6.1.

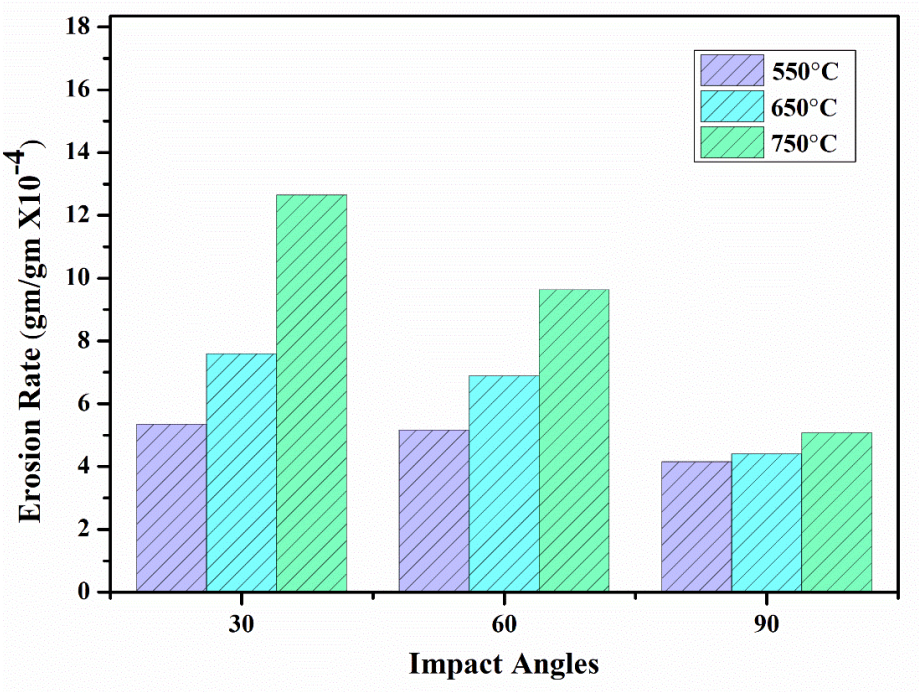

Fig. 6.10: Plot of Erosion rate vs Impact angles for corroded-eroded samples at **(a)** 550°C **(b)** 650°C, and **(c)** 750°C.

 "© ASME Publishing. Reproduced with permission. All rights reserved"

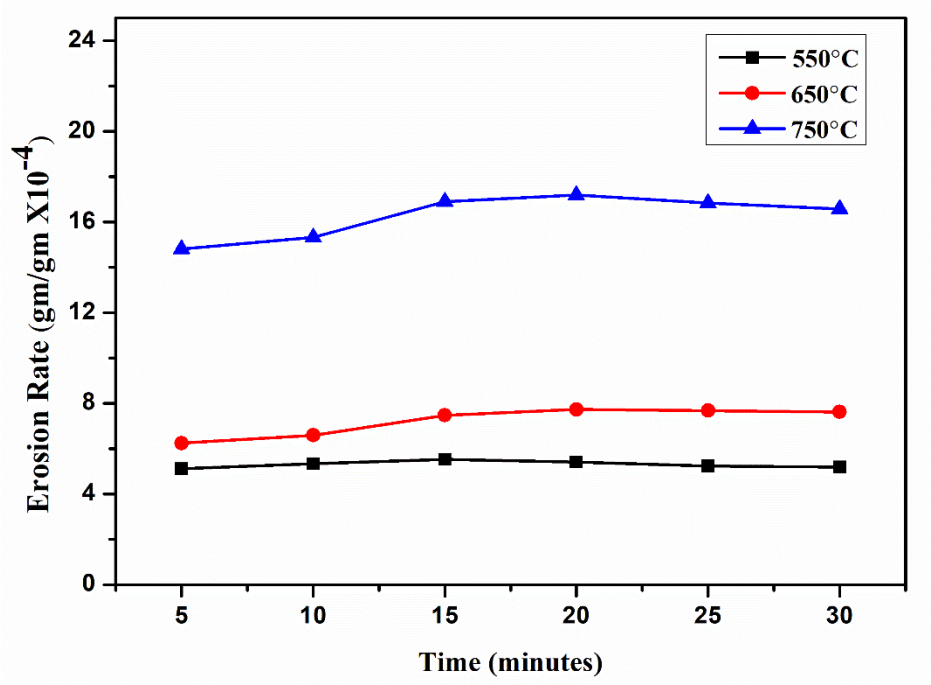

Fig. 6.11: Erosion rate vs time graph of the sample at 30° impact angle.

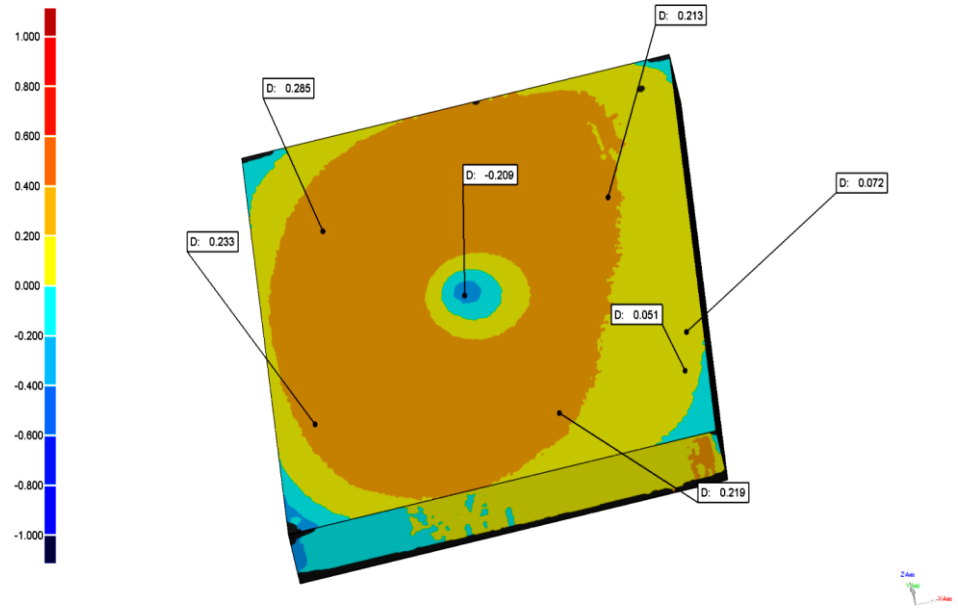

Fig. 6.12: Annotated view of Corroded-Eroded surface at 90° impact angle at 750°C.

 "© ASME Publishing. Reproduced with permission. All rights reserved"

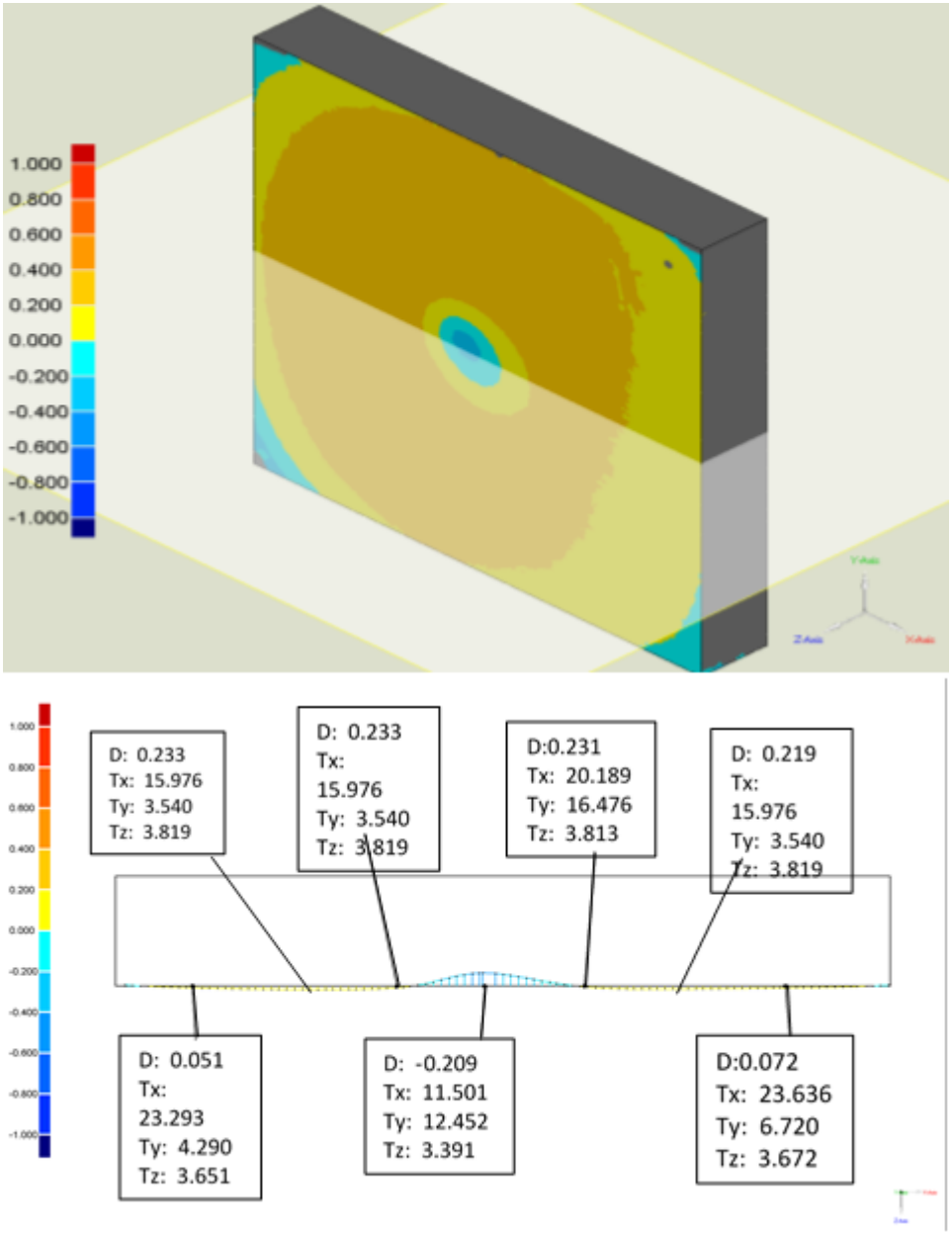

Fig. 6.13: Annotated cross-sectional view of Corroded-Eroded surface at 90° impact angle at 750°C.

SEM micrographs are taken from the center of the scar where the effect of impacting particles is clearly seen. Erosion being a complex material removal process depends on several factors, which operate in synergy, with impingement angle as the most important parameter [181]. Material removed under low impact angles with high velocity (30° and 100 m/s) conditions is largely governed by 'low angle metal cutting'

 "© ASME Publishing. Reproduced with permission. All rights reserved"

mechanism shown in Fig. 6.14(a). Along with this, the fracture of ridges around dimple formed due to particle embedment has been identified as another mode of material removal in a later stage (Fig. 6.14b).

Table 6.1: Tabulated data of Point wise depth for Corroded-Eroded surface at 90° impact angle at 750°C.

Data Points	Dev (mm)	Test-X (mm)	Test-Y (mm)	Test-Z (mm)
A001	-0.209	11.501	12.452	3.391
A002	0.233	2.255	6.587	3.833
A003	0.213	20.189	16.476	3.813
A004	0.051	23.293	4.290	3.651
A005	0.072	23.636	6.720	3.672
A006	0.285	4.028	18.715	3.885
A007	0.219	15.976	3.540	3.819

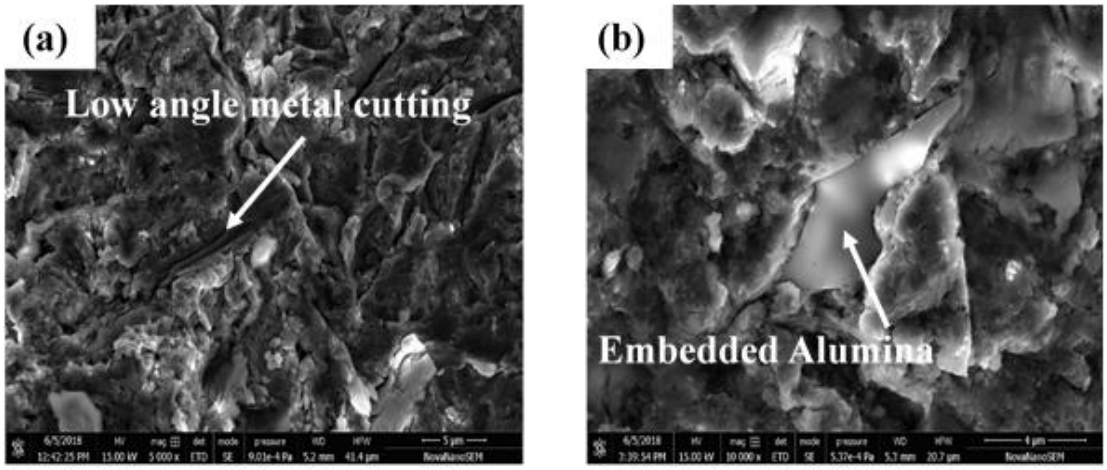

Fig. 6.14: SEM micrograph showing the scar at 30º for (a) 650°C (b) 750°C.

 "© ASME Publishing. Reproduced with permission. All rights reserved"

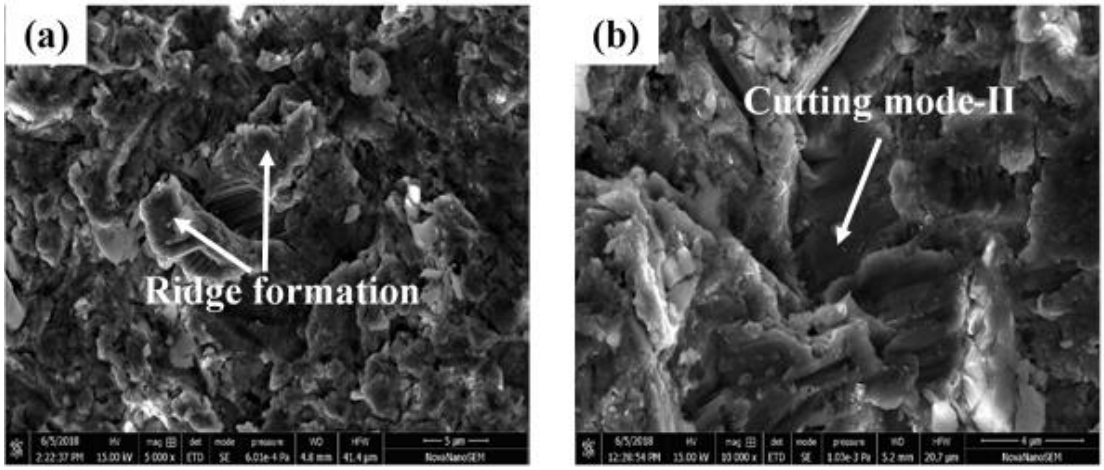

Fig. 6.15: SEM micrograph showing the scar at 60º for **(a)** 650℃, and **(b)** 750℃.

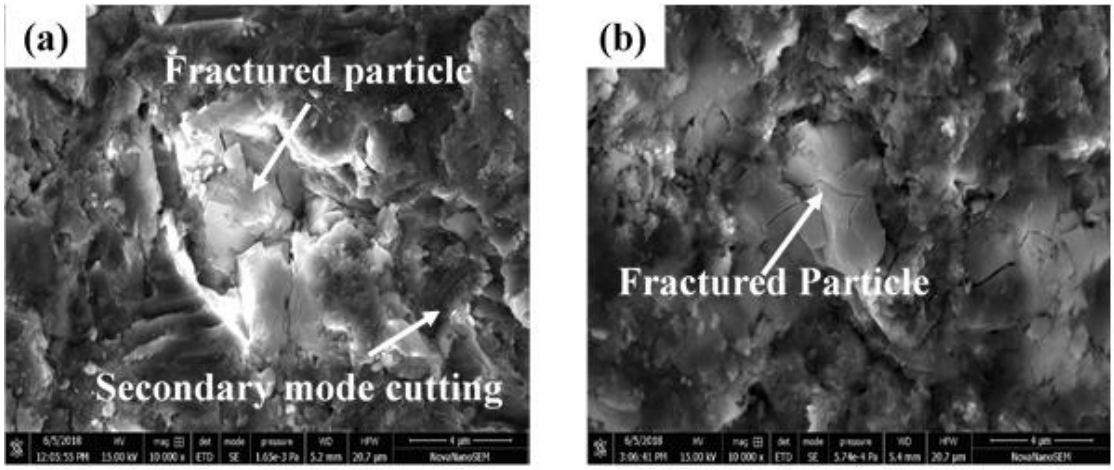

Fig. 6.16: SEM micrograph showing the scar at 90º for **(a)** 650℃, and **(b)** 750℃.

At intermediate impact angles, cutting mode II occurs. In this type of cutting, the scar is short and deep with no materials collected on sides in the form of ridges (Fig. 6.15a-b). At high impact angle and high particle velocity, fracture of embedded particle takes place due to the repeated impact of the incoming particle. In addition, secondary metal cutting is also observed, eroding a small portion of material when deflected with the already embedded particle (Fig. 6.16(a,b)). With the increase in temperature of erosion, these mechanisms are seen to be more promising. The depth of cut, lip formation and fracture of ridges are dense. Similar findings are already reported in Chapter 4.2 [176].

 "© ASME Publishing. Reproduced with permission. All rights reserved"

6.3 DISCUSSION

6.3.1 Hot- corrosion mechanism

Hot corrosion test performed at 550,650 and 750℃ for 20 h shows that at 550℃, protective layer of chromium oxide remains unbroken due to higher eutectic temperature of the salt mixture, whereas in the case of 650 and 750℃ dissolution of protective chromium oxide layer takes place [179]. The eutectic temperature of Na_2SO_4 and NaCl salt mixture is 628℃, therefore, when the samples were exposed above this temperature, the protective Cr_2O_3 layer gets broken easily and forms crevices and cracks. These cracks allow the sulfur to diffuse into the substrate through capillary effect and cause oxidation on reacting with steel substrate. The presence of Na_2SO_4 in the salt mixture used for hot corrosion, accelerates the oxidation of steel, as these are a rich source of acidic and basic flux. Figure 6.3(a-c) shows that the depth of attack is maximum at 750℃, followed by 650℃, whereas, the depth of attack is minimum in the case of 550℃. Thus, a thick passive oxide layer is formed by virtue of chlorination/sulfidation, produced by the molten salt mixture. These oxide formed layers are further responsible for the acceleration in the oxidation rate, on their reaction with the salt mixture [182]. Thereafter, rapid oxidation follows due to the reaction between oxygen and iron, forming iron oxides resulting in noticeable porosity and delaminated oxide layers. The accelerated oxidation behavior promotes the growth of oxides, which induces stress. Beyond a certain thickness, the oxide scales are incapable of bearing the induced stress, thereby, causes spalling, rumpling and bucking of scales, which is formed over the steel substrate [183]. Spalling of these scales unmasks the steel substrate, exposing directly into the air which reduces the corrosion rate (Fig. 6.1). Among the three samples coated with two salt mixture exposed at different temperatures, the sample at higher temperature exhibits maximum weight gain as compared to one exposed at 650 and 550℃ for 20 h. Surface

 "© ASME Publishing. Reproduced with permission. All rights reserved"

exposed at elevated temperature was more prone to corrosion than those exposed at the lower temperature. This is due to the formation of eutectic compounds that diffuse in the substrate because of its high fluidity at corresponding temperatures. This behaviour is in line with an earlier investigation [184].

The salt mixture in the liquid state seeps through the interface between the substrate and salt mixture. This is due to low oxygen activity at the interface as compared to the surrounding environment. This seeping of salt increases the crack size with the increase in oxidation temperature as shown in Fig 6.3a that a number of crevices and delaminated layers are formed at 750°C. With the reduction in temperature to 650°C (Fig. 6.3b), the severity of corrosion is seen to be moderate with a larger number of smaller cracks initiating from the surface. These surface cracks are seen to terminate within the corroded layer. Whereas, at 550°C (Fig. 6.3 c) negligible thickness is formed since the eutectic temperature is overhead. Thus, hot corrosion can be considered a temperature-dependent phenomenon. The products formed during corrosion are substantiated by surface morphology and composition, illustrated in Figs. 6.5-6.7. It is clear form EDS analysis that with the increase in temperature, the concentration of Fe increases and concentration of Cr decreases on top surface from 550 to 750°C. Hence, the alloying elements diffuse from the substrate to surface forming a depleted zone below the oxide scales. The SE x-ray mappings shown in (Figs. 6.8 & 6.9), illustrate the mechanism under which the depletion of chromium takes place. Since, melting of the salt mixture takes place from the interface, salt mixture attacks at the grain boundaries. At the same time, the salt elements are seen to diffuse from the surface into the substrate forming pits and voids. Except for certain regions, rich content of oxygen is present in the oxide layer and depleted layer as well. Depletion layer thickness increases with an increase in hot-corrosion temperature. This attributes to the higher diffusion coefficient of Cr as

 "© ASME Publishing. Reproduced with permission. All rights reserved"

compared to Fe. This indicated that salts react with oxides. Oxidation is extremely sensitive to the amount of chlorine and sulfur gas. Therefore, in the combined Cl-S-O atmosphere, the oxide is the final constitution of the scale due to the lowest free energy. Few reactions with two salt mixture are reported as:

$NaCl = Na^{+} + Cl^{-}$ (6.1)

$2Cr + 3/2\ O_2 = Cr_2O_3$ (6.2)

$Fe + 1/2O_2 = FeO$ (6.3)

$FeO + Cr_2O_3 = FeCr_2O_4$ (6.4)

$3Fe + 2O_2 = Fe_3O_4$ (6.5)

$2Fe + 3/2O_2 = Fe_2O_3$ (6.6)

$Na_2O + Cr_2O_3 = 2NaCrO_2$ (6.7)

$Fe + Cl_2 = FeCl_2$ (6.8)

$Cr + S^{2-} = CrS$ (6.9)

$5CrS + 3S^{2-} = Cr_5S_8$ (6.10)

$Fe + 2S^{2-} = FeS_2$ (6.11)

Under isothermal hot-corrosion, oxides are formed initially, thereafter, chlorine gas may be liberated by dissociation of NaCl into Na^{+} and Cl^{-} ions. Of these, Cl^{-} ions seep into the interface and react with the substrate, forming metal chlorides such as $CrCl_2$ and $FeCl_3$. NaCl present over the surface reacts with oxides to form $FeCr_2O_4$ and Cl_2 gas. The evaporation of this Cl_2 gas leads to the formation of crack/pits. Cross-section of each sample showed oxide layers, chromium depleted regions and cracks/pits (Fig. 6.3(a-c))**.** In addition, the non-protective Cr_2O_3 layer formed over the substrate is seen to peel off from the surface, which illustrates that the layers are non-adherent and weak. Based on the standard free energy of formation of oxides, Cr and Fe strive to form oxides at metal/salts interface. The standard Gibbs free energy of formation of different phases

 "© ASME Publishing. Reproduced with permission. All rights reserved"

formed during the course of hot corrosion reaction at 650 and 750°C are given in Table 6.2. Therefore, it is concluded that oxidation, chlorination, and sulfidation have been identified as the processes responsible for hot corrosion.

Table 6.2: Standard Gibbs Free Energies of product formation at 650 and 750°C [185].

Products formed	ΔG_T (KJ/mol) [A + BT log T + CT]	
	at 650°C	at 750°C
Cr_2O_3	-880.31	-854.37
$FeCr_2O_4$	-457.15	-447.03
$FeCl_2$	-229.91	-218.61
Fe_3O_4	-196.74	-184.22
Fe_2O_3	-119.62	-105.73
FeS_2	-15.188	+22.58

6.3.2 Pre-hot corrosion erosion mechanism

Erosion is a complex material removal process in which the properties of erodent, conditions of impact and properties of target material play a crucial role. In this investigation, the effect of hot corrosion causing enhancement in the loss of material has been studied. SEM micrographs of the corroded surfaces, (Fig. 6.5-6.7), reveal brittle corrosion products and spalling of the weakly adherent layers formed by virtue of hot corrosion, under the effect of corrosion attack by chloride and sulfide ions. As a result, a non-protective and non-adherent layer is formed in combination with some protective adherent layer [186]. These layers when impacted with high kinetic energy, get easily fractured and shredded resulting in higher mass loss initially.

 "© ASME Publishing. Reproduced with permission. All rights reserved"

Considering the effect of impact velocity, the kinetic energy associated with abrasive particle increases with impact velocity. Such a high kinetic energy of impact creates higher shear stress on the surface. The material is unable to resist such a high shear force and therefore suffers severe material loss. Along with spalling and shredding, localized fractures and cutting has been identified as corrosion enhanced erosion mechanism. A localized fracture occurs by extruded lips which transform into flattened platelets on the continuous impact of abrasive particles striking over the pre hot corroded surface during erosion [157].

The erosion rate was seen to increase many folds due to corrosion. Corrosive species on reacting with the substrate breaks the protective layer and form deleterious products of corrosion. These products are weak and form a non-adherent layer on the surface. The resistance to kinetic energy of impact being low, these weak layers undergo high material loss. With subsequent impact, crack is developed in the deformed layer formed under corrosion. These cracks propagate removing the weak formed layers and fresh metal is exposed. The steel substrate, therefore, offers higher resistance to the impact particle and therefore the erosion rate is seen to decrease with further increase in the duration of impact. Another consequence of high particle impact is the development of microcracks on the surface, which progresses further to form delamination. These delaminated layers shown in Fig. 6.3(a) are responsible for the removal of material in chunks and cause a random increase in erosion.

Obeying the dictates of impingement angle, metal removal under low impact angles and high-velocity conditions is controlled by ‘low angle metal cutting’ mechanism (Fig. 6.14). The tangential component of velocity vector helps in achieving the critical energy required by the particle to remove material in the form of small metallic chips. While the normal component of velocity helps the particle to embed into the surface. The

 “© ASME Publishing. Reproduced with permission. All rights reserved”

impacting particle creates dimples and forms ridges on the surface in course of removing the metallic chips. The multiple impacts due to incoming stream of abrasive particle fracture these ridges and can be thought of as 'secondary mode' of material removal. At an intermediate angle of impact, removal of material takes place mainly by cutting mode II mechanism (Fig. 6.15) however, other mechanisms like secondary mode of cutting also have a marked influence. Since no material is seen to collect on sides in the form of ridges, therefore, fracture and flattening are absent. On the other hand, chips attached to the end of the scar are susceptible to further impact. With an increase in the angle of impingement the normal component of the velocity vector is seen to increase, hence, at the normal impact of 90° the particles are seen to be embedded deep into the surface. These particles suffer the subsequent impact of the high-velocity particle and suffer fracture (Fig. 6.16). Consequently, they are removed from the surface forming lips, which gets flattened and fractures with the course of impact. The embedded particles are also responsible for secondary metal cutting which is significantly seen due to the deflection of the incoming particle on striking with already present ones.

The erosion rate changes significantly with the increase in temperature. This is due to the deleterious product formed during hot corrosion, which is detrimental to the surface properties of the material. As already discussed, the products of corrosion at 750℃ are more harmful than the products formed at 650℃. Whereas, 550℃ shows an insignificant effect on surface degradation. Owing to this, these products are easily spalled off the surface and thereby, expose the substrate material directly to the impacting particle. These directly exposed surfaces suffer different rates of material removal with an increase in temperature, which has been explained by the change in properties of the material with an increase in temperature [176].

 "© ASME Publishing. Reproduced with permission. All rights reserved"

6.4 CONCLUSIONS

Effect of pre-hot corrosion on the Type 446 stainless steel by the salt mixture of $75Na_2SO_4 + 25NaCl$ (wt.%) is studied on its erosion behaviour, at different temperatures of 550, 650 and 750℃. The conclusions drawn from this study are as follows:

1. The hot corroded samples exposed to 550℃ has a golden grey surface appearance with very little scaling, while at 650℃, the appearance is dark reddish-brown with spalling of the scale. The surface appears to be dim-grey in colour with heavy spalling of fragile scale when exposed to 750℃.
2. Evaporation of chlorides during the process of hot corrosion led to the formation of pits/cracks in the two salt mixture ($75Na_2SO_4$ /25NaCl) deposited sample when exposed at 650 and 750℃ for 20 h.
3. Lower erosion resistance of the pre-hot corroded samples from the two salt mixture when tested at 650 and 750℃ for 20 h, is attributed to crevices/cracks formation and delamination of weakly bonded layer leading to high erosion rate.
4. The erosion rate is inversely proportional to angle of impact, due to lower resistance offered by the material to the shear force acting at high velocity of impact.
5. Morphology of the scars is more promising to justify the mechanism of erosion. The fracture of embedded particles, the crests, and plough marks are more intense with the increase in temperature.

 "© ASME Publishing. Reproduced with permission. All rights reserved"